Heliyon 11 (2025) e41064

Contents lists available at ScienceDirect

Heliyon

journal homepage: www.cell.com/heliyon

Research article

Fabrication of biocidal materials based on the molecular interactions of tetracycline and quercetin with hydroxyapatite via *In Silico*- and In vitro approaches

Anastasiia M. Isakova [a], Maxim A. Kutyrev [a], Aleksandra S. Kudasheva [a], Elizaveta V. Rogacheva [b], Lyudmila A. Kraeva [b], Sergey Shityakov [a], Mikhail V. Zhukov [a], Sviatlana A. Ulasevich [a,*], Ekaterina V. Skorb [a,**]

[a] *Infochemistry Scientific Center, ITMO University, Lomonosova str. 9, 191002, Saint Petersburg, Russia*
[b] *Pasteur Institute of Epidemiology and Microbiology, 14 Mira Street, 197101, Saint Petersburg, Russia*

ARTICLE INFO

Keywords:
Hydroxyapatite
Drug adsorption
Binding constant
Molecular docking
Antimicrobial activity

ABSTRACT

Synthetic hydroxyapatite (HA) materials with antibacterial and biocompatible properties have potential for biomedical applications. The application of various computational methods *in silica* is highly relevant for the optimal development of modern materials. In this work, we used molecular docking to determine the binding constants of tetracycline (TET) and quercetin (QUE) with hydroxyapatite and compared them to experimental data of the adsorption of tetracycline (TET) and quercetin (QUE) on the HA surface. The experimental adsorption study was performed via the UV–VIS method. The fabricated biocidal powders were characterized via X-ray powder diffraction (XRD), Fourier transform infrared (FTIR) spectroscopy, and scanning electron microscopy (SEM). The electrical charge of the HA particle surface was determined via zeta potential measurements. The molecular docking method was used to predict the binding affinities of TET and QUE for HA. We also performed molecular docking studies to predict the binding affinity of TET and QUE for HA. These affinities correlate with the experimental binding constants, suggesting that molecular docking is a good tool for material property prediction. In addition, the antimicrobial activity of the HA/TET and HA/QUE powders was determined against 2 g-positive bacterial strains: *S. aureus* and *E. faecalis*. The obtained HA powders were evaluated for biocompatibility in vitro with the myoblast cell line C2C12.

1. Introduction

The demand for multifunctional materials, which regulate their physicochemical and biomechanical properties, have therapeutic effects, etc., is high in all areas of science and technology [1–4]. To effectively use such materials for their intended purpose, various aspects of the interaction of their constituent parts need to be studied in more detail: changing the crystal structure and surface charge, determining binding constants, and finding the most favorable spatial conformation [5–8].

Bone tissue engineering is an advanced approach to the development of functional scaffold materials for repairing and regenerating

* Corresponding author.
** Corresponding author.
E-mail address: saulasevich@itmo.ru (S.A. Ulasevich).

https://doi.org/10.1016/j.heliyon.2024.e41064
Received 12 July 2024; Received in revised form 4 December 2024; Accepted 6 December 2024
Available online 9 December 2024

damaged bones [9]. A major research direction in this field is to produce scaffolds with desirable shapes, structures, and physical, chemical, and biological features [10]. Hydroxyapatite (HA), a main inorganic component of bones and teeth, is one of the most promising materials in bone tissue engineering [11]. Owing to its biocompatibility, biodegradability, and good adsorption properties, HA has been widely used in the repair of hard tissues and drug delivery [12,13]. However, HA has lower properties than natural bones do, so it is necessary to improve HA-based materials by adding other components [14]. For example, poor antibacterial activity can easily cause bacterial infection and chronic inflammation, eventually resulting in implant failure [15]. Unfortunately, research findings have shown that pure HA has a low ability to deactivate bacteria [16]. As a result, additional components are needed to improve antibacterial activity and maintain biocompatibility. The addition of bioactive phytochemicals such as flavonoids can also inhibit osteoclastogenesis, prevent bone resorption and bone loss, or promote bone formation via the promotion of osteoblast genesis [17].

Tetracycline (TET) is one of the most effective antibiotics and the second most common antibiotic worldwide. It has a broad spectrum of activity and has been extensively used in medical applications to prevent bacterial infections [18]. Quercetin (QUE), a plant flavonoid, notably enhances osteoblast proliferation, differentiation, and mineralization, whereas osteoclast cell proliferation and differentiation are dramatically suppressed by it [19]. Thus, HA-based biomaterials modified with these substances have good prospects for use in tissue engineering. Despite many articles in which various properties of the HA/TET and HA/QUE systems are considered [20–25], further investigations are still needed. In particular, few scientists have resorted to the use of theoretical methods to study the interaction of HA with substances and compared the obtained results with experimental data. However, modern theoretical chemistry is a powerful tool that can provide insights into many phenomena and processes in chemical systems, increasing the efficiency of their use in practice.

In this regard, this study aims to apply molecular docking studies for the prediction of the binding affinity of TET and QUE to HA and the fabrication of biocidal materials based on HA particles adsorbed on the surface of TET and QUE molecules. The novelty of our approach lies in combining theoretical calculations and confirming them with experimental data as the gold standard. Notably, the calculated binding affinity constants of tetracycline and quercetin to the hydroxyapatite surface via molecular docking are correlated with experimental data obtained in the laboratory. UV–VIS spectroscopy was used as a standard experiment to confirm the calculations. In addition, the antibacterial activity of the prepared biocidal HA powders was tested against the bacterial strains *S. aureus* and *E. faecalis*, which are the main causative agents of osteomyelitis and other bone diseases [26,27]. Biocompatibility was evaluated through in vitro experiments in the presence of the C2C12 mouse myoblast cell line. We also performed molecular docking studies to predict the binding affinity of TET and QUE for HA. The molecular docking results were also compared with the experimental binding constants determined via the UV–VIS spectrophotometric method.

2. Materials and methods

2.1. Materials

Tetracycline hydrochloride ($C_{22}H_{24}H_2O_8{\cdot}HCl$, ≥99.9 %) was purchased from Fisher BioReagents (Thermo Fisher Scientific Inc., Pittsburgh, Pennsylvania, USA). Quercetin dihydrate ($C_{15}H_{10}O_7{\cdot}2H_2O$, ≥98.9 %) and acridine orange were obtained from Vecton (Vecton Corp., Saint Petersburg, Russia). Propidium iodide (PI) was obtained from Invitrogen™ (Burlington, Canada). Fetal bovine serum (FBS), Dulbecco's modified Eagle's medium (DMEM), and penicillin/streptomycin were purchased from BioloT (BioloT Ltd., Saint Petersburg, Russia).

2.2. Synthesis of HA powder

Hydroxyapatite (HA) powder was synthesized according to the literature via a sol–gel method [28]. Briefly, an aqueous solution of 0.3 mol/mL NaH_2PO_4 was added dropwise to a 1.4 mol/mL $CaCl_2$ solution at room temperature. To control the pH of the solution, NH_4OH was also added in a dropwise manner. After the addition was completed, the solution was maturated for 60 min and centrifuged. The as-precipitated HA was oven-dried overnight at 60 °C. The powders were sifted, and a fraction of particles with a size of 81 μm was used.

2.3. Adsorption experiments

The adsorption study was conducted by adding 10 mg of HA powder to different tubes containing 1.5 mL of tetracycline and quercetin ethanol solutions at different concentrations (1, 10, 100, or 1000 μg/mL) with 10-fold dilutions and shaking in IKA mini G (IKA-Werke GmbH & Co. KG, Staufen im Breisgau, Germany) at 1610×*g* for 5–10 min at room temperature. After mixing, the supernatants were collected, and the powders were dried in an oven at 60 °C for 3 h. For the kinetics studies, solutions at initial concentrations of 10 μg/mL were used. The substance concentration was then analyzed at different time points. The time required for the adsorption of TET and QUE was estimated by decreasing the absorbance peaks in the UV–VIS spectra. The amount of adsorbed biologically active compounds (q_e, μg/mg) and the adsorption rate (%) at the equilibrium state were obtained as follows:

$$q_e = \frac{(C_0 - C_e)V}{m} \quad (1)$$

$$\%Adsorbed = \frac{(C_0 - C_e)}{C_0} \bullet 100 \quad (2)$$

where q_e (μg/mg) is the adsorption amount; C_0 and C_e (μg/mL) are the initial and equilibrium concentrations of the substance in solution, respectively; V (mL) is the volume of the substance solution; and m (μg) is the weight of the adsorbent.

2.4. Characterization method

The HA particle morphology was characterized via a scanning electron microscope (Tescan Vega 3) equipped with an energy dispersive X-ray (EDX) attachment (TESCAN GROUP, a.s., Brno, Czech Republic). An Au film was sputtered onto the samples to enhance conductivity via SPI sputter installation (Structure Probe, Inc., West Chester, PA, USA). The local qualitative elemental compositions of the samples were identified via energy dispersive X-ray analysis. The measurements were carried out with secondary electrons at a voltage of 20 kV. In addition to the conventional SEM image and the local qualitative elemental composition spectra, detailed maps of the elemental distribution were also generated to estimate the allocation of the elements.

Adsorption studies were carried out via a microvolume UV–visible spectrophotometer (Bioevopeak SP-MUV1000; Bioevopeak Co., Ltd., Jinan, Shandong, China) in the range of 190–850 nm. The droplet size was 2 μl. The residual amount of the drug in the solution was quantified at 240 nm for TET and 241 nm for QUE. The drug solution in ethanol with an initial concentration of 10 μg/mL was used as a baseline.

X-ray analysis of the obtained powders was carried out via CuKα radiation (λ = 1.5406 Å) on a D2 PHASER (Bruker, Billerica, Massachusetts, USA) with a 2θ range from 10 to 50° and a step size of 0.02. Tetracycline and quercetin powders were used as controls.

The presence of functional groups in pure HA and after the adsorption of tetracycline and quercetin on the HA surface were analyzed via Fourier transform infrared (FTIR) spectroscopy on an FSM 2201/2202 spectrometer (Infraspek Ltd., Saint-Petersburg, Russia). FTIR spectra of the materials were recorded in transmittance mode via KBr pellets over the wavenumber range of 500–4000 cm^{-1} at a resolution of 4 cm^{-1}. For each spectrum, 30 scans were performed. The mass ratio of the test substance to KBr was 1:100.

The zeta potential of each sample was determined via a ZetaSizer Compact-Z (Photocor Ltd., Moscow, Russia). Measurements were performed in ethanol solutions.

2.5. Antibacterial activity

The antimicrobial activity of the biocidal powders was investigated against the growth of the following pathogens: *Staphylococcus aureus* (ATCC 25912) and *Enterococcus faecalis* (ATCC 29812) microbial strains. The antimicrobial assays were performed according to 0.5 McFarland standard microbial cultures. The experiments to evaluate the antibacterial properties were performed according to the recommendations of the Clinical and Laboratory Standards Institute (CLSI) [29] and the European Committee on Antimicrobial Susceptibility Testing (EUCAST) [30]. Mueller–Hinton (MH) agar and Columbia agar containing 5 % sheep blood were sterilized by autoclaving at 121 ± 2 °C and 103 ± 5 kPa for 30 min. Warm medium (20 mL) was poured into Petri dishes (Nunc Inc., Roskilde, Denmark) and allowed to cool at ambient temperature. Inocula for MICs were prepared in sterile Mueller–Hinton broth (Oxoid). The microorganisms were grown at 37 °C for 24 h. The analysis was carried out in five experiments for each of the analyzed samples. Afterward, the samples were inoculated with 1.5 mL of microbial suspension at a density of 1×10^8 CFU/mL, prepared in phosphate-buffered saline (PBS), and incubated for 24 h. Then, 5 μL of each of the tested HA powders was applied in 3 repetitions and incubated on MH agar media for 24 h at 37 °C.

2.6. Cell culture

The C2C12 mouse skeletal myoblast cell line was purchased from Sigma Aldrich (Merck KGaA, Darmstadt, Germany and Sigma–Aldrich Co., LLC, St. Louis, Missouri, USA) and cultured in high-glucose DMEM containing 10 % fetal bovine serum (FBS) and 1 % penicillin/streptomycin at 37 °C and 5 % CO_2 in humidified (95 %) air. The culture medium was changed every 3 days. The culture medium was subsequently removed, and the cells were detached from the surface of the 75 cm^2 cell culture flask with 1 mL of 0.25 wt% trypsin solution. To neutralize the trypsin, 5 mL of the culture medium was added.

2.7. Acridine orange/propidium iodide staining

The C2C12 myoblast cell line was treated with biocidal powders (1 g/mL) at 1×10^4 cells/well in a 12-well culture plate. An aliquot of 20 μL of acridine orange (AO) stock solution (1 mg/mL) was added to each well with PBS and cooled at +4 °C. Then, an aliquot of 20 μL of propidium iodide (PI) stock solution (1 mg/mL) was added to each well and incubated in the dark for 10 min at +4 °C. The fluorescence was measured via a confocal microscope (Leica DMi 8, Germany) with an excitation wavelength of 460 nm, an emission wavelength of 650 nm for AO, an excitation wavelength of 525 nm and an emission wavelength of 595 nm for PI.

2.8. Experimental binding constant

For calculations of the experimental binding constants, we used the radioligand binding assay method. The residual concentration

of the biologically active compound (TET or QUE) in the solution at time t was calculated via the following equation:

$$C_t = \frac{A_t}{A_0} \bullet C_0 \tag{3}$$

where C_0 and C_t are the initial and residual concentrations and where A_0 and A_t are the absorbance values at time zero and time t, respectively. The absorbance values were retrieved from the highest absorbance peaks (240 nm for TET and 241 nm for QUE). The time t changed from 0 to 530 min when the adsorption process reached equilibrium. Since the experiment was conducted 3 times, the mean and standard deviation were calculated for each C_t value. The resulting mean values were input into GraphPad Prism 9.5.1 software, and the dissociation rate constants were obtained through the one-phase exponential decay equation:

$$Y = (Y_0 - NS) \bullet exp\,(-K_d \bullet X) + NS \tag{4}$$

where Y_0 is the binding at time zero, in units of the Y axis; NS is the binding (nonspecific) at infinite times, in units of the Y axis; and K_d is the dissociation rate constant in inverse units of the X-axis. The binding constants, or association constants, of TET and QUE to HA were obtained as the inverse of the respective dissociation constants via the following equation:

$$K_a = \frac{1}{K_i} \tag{5}$$

where K_a and K_i are the association and inhibition rate constants, respectively [31].

2.9. Molecular docking

The 3D coordinates of the TET (CID 54675776) and QUE (CID 5280343) molecular structures were retrieved from the PubChem database as 3D SDF files. The HA structure was generated via the HA unit cell CAR file, which is available from the INTERFACE-MD software developed by the Heinz group at the University of Colorado at Boulder. The HA unit cell consists of six PO_4^{3-} groups, two OH^- groups, and ten Ca^{2+} ions. The HA slab was designed via the TopoTools v.1.8 VMD plugin. Molecular docking was performed via the AutoDock and AutoDock Vina (ADVina) programs with default settings. Genetic and gradient optimization algorithms were employed. The ligand-HA binding site at the HA center for each ligand-HA complex was identified via Cartesian coordinates: x = 9.2 Å, y = 15.94 Å, and z = 3.52 Å. Grid maps were created with a grid spacing of 0.375 Å and a dimension size of 60 Å. To prepare the structures for molecular docking, Gasteiger partial charges were assigned, and rotatable bonds were defined according to standard protocols published elsewhere. The docking output results were represented by the approximation function as the estimated Gibbs free energy of binding (ΔG_{bind}).

2.10. Statistical analysis

All experiments were reproduced at least three times using three samples from each group. The obtained data were averaged with the standard error of the mean. Statistical analysis to compare the results of the cell antibacterial activity and cell viability assays was performed via ANOVA (*p < 0.05).

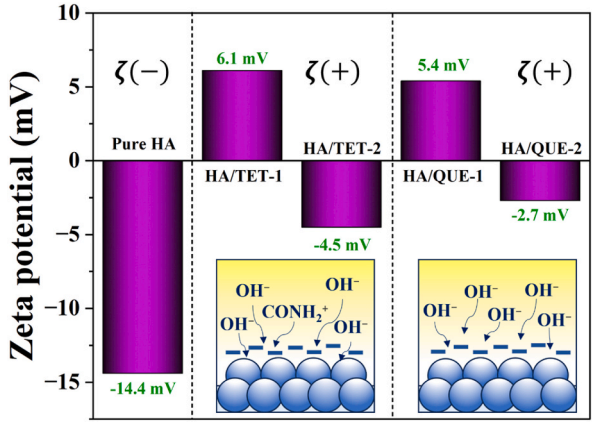

Fig. 1. Zeta potentials of pure HA, HA with tetracycline (HA/TET-1, HA/TET-2), and HA with quercetin (HA/QUE-1, HA/QUE-2). HA/TET-1, HA/TET-2, HA/QUE-1, and HA/QUE-2 indicate that tetracycline and quercetin ethanol solutions were used at 1 mg/mL and 100 μg/mL, respectively.

3. Results and Discussion

3.1. Characterization of synthesized materials

To estimate the possibility of antibiotic adsorption on HA particles, the surface charge of HA particles was initially measured. Fig. 1 shows the results of the surface charge and zeta potential measurements of the HA particles after antibiotic adsorption at 25 °C. As shown in Fig. 1, the initial surface charge of HA is negative and equal to −14.4 mV. Notably, the negative value of the zeta potential correlates with literature data for hydroxyapatite powders synthesized in aqueous solutions [32–35]. In addition, the zeta potential of natural bone-derived HA particles was found to be −9.25 ± 0.9 mV at a typical physiologic pH of 7.4 [36]. The negative values of the zeta potential are suggested to have a significant favorable effect on the attachment and proliferation of bone cells [36]. The adsorption of tetracycline from an ethanol solution led to a significant change in the surface charge to +6.1 mV (Fig. 1, plot for HA/TET-1). However, the changes in the HA surface charge and zeta potential value in the less concentrated solutions (the tetracycline concentration was 100 μg/mL) were smaller. The surface charge of the HA/TET-2 particles remains negative and equal to −4.5 mV (Fig. 1, plot for HA/TET-2). The decrease in or change in the zeta potential in the presence of TET may be caused by the lower adsorption of TET on the surface of HA, the greater adsorption of the antibiotic and the thick adsorption layer. The interaction between the negatively charged tetracycline and quercetin with the negatively charged HA is probably due to the interaction of the functional groups of the adsorbed molecules with the hydroxyl groups of the HA surface [31]. This explains the noticeable reduction in the zeta potential of HA particles with adsorbed TET. A higher adsorption level of TET considerably changes the surface charge and zeta potential of HA. Notably, tetracycline has a protonated form via NH_2 groups at the fourth carbon atom in concentrated solutions. It determines the positive charge of a molecule. An increase in the amount of adsorbed TET also increases the number of NH_3^+ groups at the interface that react with the surface of the HA. The positive charge originating from these groups has a direct effect on lowering the negative charge and zeta potential of HA in the presence of TET, as demonstrated in the present study.

The XRD profiles of pure HA and powders after adsorption of tetracycline (HA/TET-1) and quercetin (HA/QUE-1) are shown in Fig. 2A. In all XRD patterns (Fig. 2 A, plots 1–3), there are peaks at 2Ɵ: 25.9°, 31.879°, 32.232°, 32.917°, 34.14°, 39.91°, 46.75°, and 49.53°. These peaks correspond to the main Miller planes and correspond to HA crystal angles of 25.879° (002), 31.774° (211), 32.197° (112), 32.902° (300), 34.049° (202), 39.819° (310), 46.713° (222), and 49.469° (213) according to ICDD-PDF# 9–432 and literature data [18,36–38]. The characteristic peaks of tetracycline and quercetin were not detected at 10–50° in the HA/TET-1 and HA/QUE-1 composites, respectively. This could be related to the amorphous structure of tetracycline and quercetin [38,39]. Owing to this phenomenon, samples (HA/TET-2 and HA/QUE-2) obtained from less concentrated solutions are not included in Fig. 2B. In addition to zeta potential measurements, FTIR analysis was used to estimate the possibility of adsorption of tetracycline and quercetin on HA or binding between HA particles and tetracycline or quercetin.

Fig. 2B shows the FTIR spectra of the pure HA, HA/TET-1, and HA/QUE-1 composites. In the spectra of all the samples, there are two intense peaks at 2355 cm^{-1}, and those at 3740 cm^{-1} are associated with OH^- groups [40]. The peak at 1049 cm^{-1} is attributed to PO_4^{3-} vibrations [41]. The two peaks at 1427 cm^{-1} and 1462 cm^{-1} are associated with CO_3^{2-} impurities [42]. The PO_4^{3-} peak decreases with increasing content of tetracycline in HA, whereas a strong peak attributed to the OH^- group at 2355 cm^{-1} [43,44] can be observed in all the samples (Table 1). To study the interaction between the hydroxyapatite surface and the adsorbed molecules, we deconvoluted the FTIR spectra (Fig. 2C–H). Deconvolution of the spectra separates overlapping bands in the $\upsilon_4PO_4^{3-}$, $\upsilon_2CO_3^{2-}$, $\upsilon_3CO_3^{2-}$ and amide regions, allowing a more detailed analysis of changes at the atomic level [45]. The PO_4^{3-} peak is deconvoluted into two peaks, which could be due to its overlap with the HPO_4^{2-} apatite peak. Usually, separating these peaks and distinguishing them from each other by colorimetry are very difficult [45]. Fig. 2C–H shows that the intensity of the OH^- band vibration is lower in the HA/QUE-1 and HA/TET-1 composites than in pure HA. This may be due to the interaction and formation of hydrogen bonds between TET or QUE and the hydroxyapatite surface. The interaction of positively (protonated form) charged tetracycline and quercetin with

Table 1
Comparison of the bands observed in the FT-IR spectra of the samples with the literature data

Sample	Domain, Assignment	IR (cm^{-1})	Reference
Pure HA	$\upsilon_3PO_4^{3-}$ and HPO_4^{2-} symmetric and asymmetric stretching	1052, 1101	41
HA/TET-1		1052, 1096	
HA/QUE-1		1054, 1097	
Pure HA	$\upsilon_2CO_3^{2-}$ type A1 doublet	1531	40
HA/TET-1		1531	
HA/QUE-1		1530	
Pure HA	H_2O bending	1694	3,4, 40
HA/TET-1		1693	
HA/QUE-1		1693	
Pure HA	H_2O	3290	40
HA/TET-1	Symmetric stretching	3269	
HA/QUE-1		3282	
Pure HA	OH^- stretching	3741	40, 43, 44
HA/TET-1		3738	
HA/QUE-1		3739	

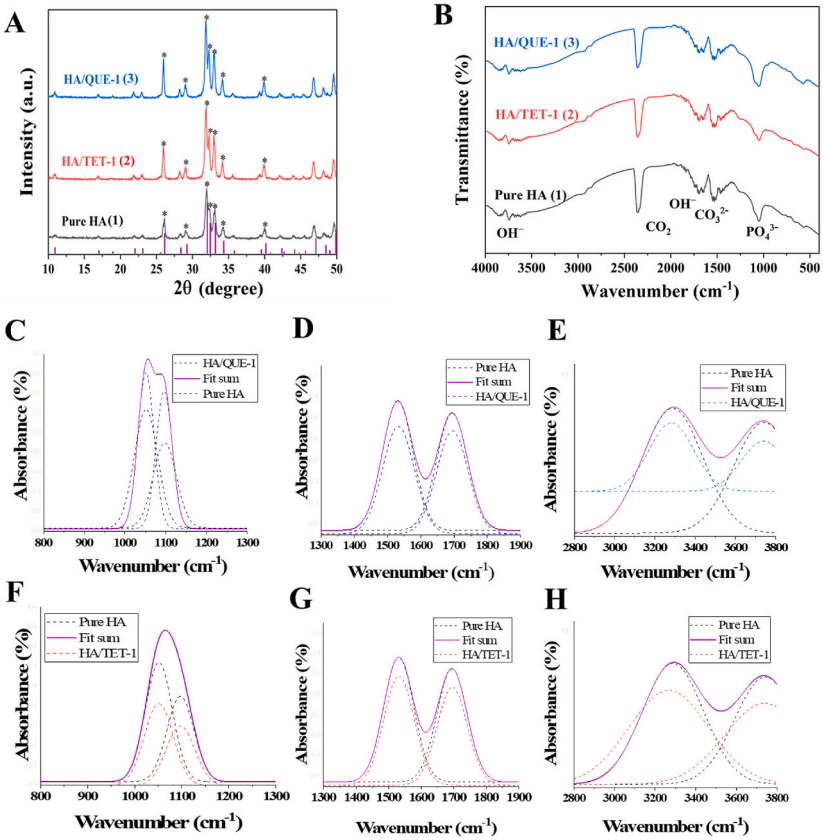

Fig. 2. A) XRD profiles of pure HA particles (plot 1), HA/TET-1 (plot 2) and HA/QUE-1 (plot 3). HA/TET-1 and HA/QUE-1 indicate that tetracycline and quercetin ethanol solutions, respectively, were used at a concentration of 1 mg/mL. The HA peaks with intensities greater than 15 % are highlighted as (*). B) FTIR spectra of pure HA particles (plot 1), HA/TET-1 (plot 2) and HA/QUE-1 (plot 3). C–H) Deconvolution of pure HA and HA/QUE-1 (C), pure HA and HA/TET-1 (F) showing the $\upsilon_4PO_4^{3-}$ and HPO_4^{2-} bands (800–1300 cm^{-1}). Deconvolution of the $\upsilon_3CO_3^{2-}$ band (1300–1900 cm^{-1}) for 80 °C dried pure HA and HA/QUE-1 (D), pure HA and HA/TET-1 (G). Deconvolution of the a_1H_2O and a_1HO^- bands (2800–3800 cm^{-1}).

negatively charged HA is probably due to the interaction of the functional groups of the adsorbed molecules with the hydroxyl groups of the HA surface [44].

In addition, in a plot of the HA/QUE-1 composite, we also observed an increase in peak intensity at approximately 570 cm^{-1}, which is responsible for the C−H bending of aromatic hydrocarbons (out-of-plane) [43]. Thus, we can assume that tetracycline and quercetin, which have aromatic groups, are adsorbed on the HA surface.

The surface morphology of pure HA was analyzed via SEM and is shown in Fig. 3A–G. The pure HA particles are roundish conglomerates of *ca.* 20–40 μm. The conglomerates consist of hexagon-shaped structures. The surface of the particles is smooth, and the diameter of the pores is approximately 100 nm. Elemental mapping analysis revealed calcium and phosphorous in the pure HA, HA/TET-1 and HA/QUE-1 powders (Fig. 3H–J). A uniform distribution and good dispersion of Ca, P, O and C throughout the surface of the HA were observed. The quantitative chemical compositions of HA/TET-1 and HA/QUE-1 were estimated from EDX (Table 2). The EDX spectra presented in Fig. 3 K−M reveal that the pure HA, HA/TET-1 and HA/QUE-1 composites are composed of four main elements, Ca, P, O and N. The presence of the N constituent element from the tetracycline in the HA/TET-1 powder was statistically significant. Therefore, we did not include nitrogen in the results. EDX analysis revealed that the Ca/P ratio in the samples varied from 1.7 for pure HA to 1.61 ÷ 1.67 for the HA/TET-1 and HA/QUE-1 composites. Thus, we can assume a high stoichiometry of hydroxyapatite [46].

However, we indirectly determined the presence of adsorbed tetracycline and quercetin molecules in the sample. The HA/TET-1 and HA/QUE-1 composites were soaked in distilled water for 24 h, and then, the resulting solutions were analyzed via the UV–VIS method. The resulting composites released tetracycline and quercetin when kept in solution.

3.2. Adsorption kinetics studies

The adsorption of tetracycline and quercetin on the HA powders was also confirmed via the UV–VIS method. UV–VIS spectroscopy revealed a peak at approximately 240 nm in the spectra of HA/TET-1 and HA/QUE-1. A weaker peak at 377 nm was also observed in the case of free quercetin (Fig. 4A and D). The diluted solutions of tetracycline and quercetin were used to determine the binding

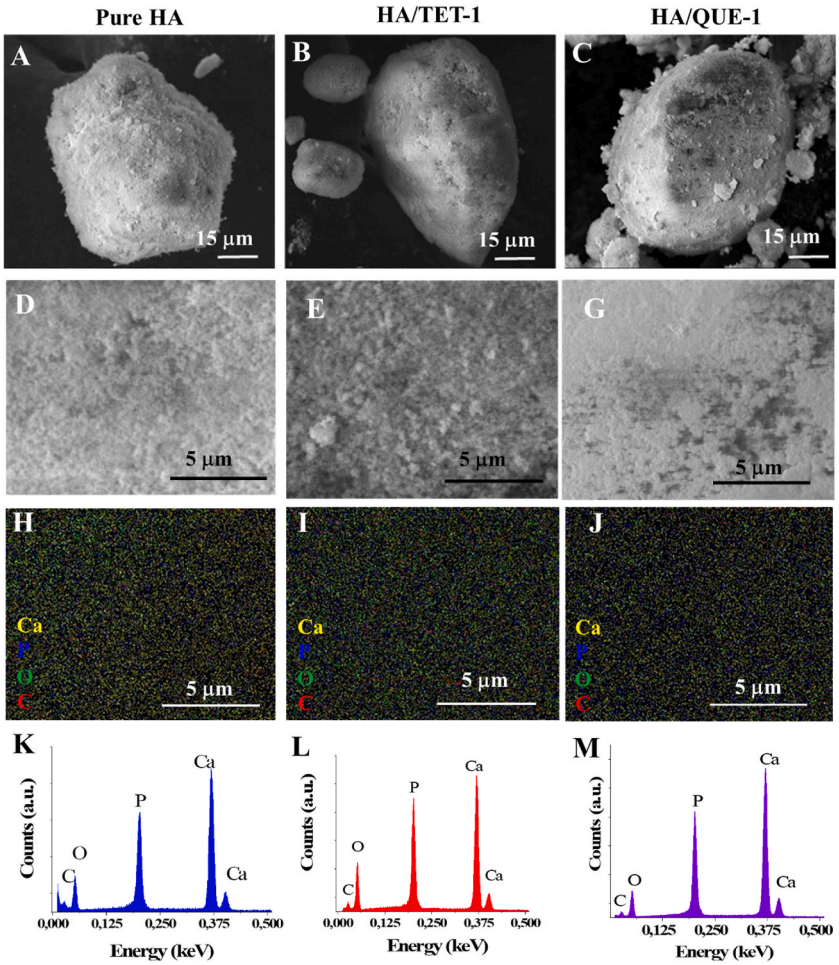

Fig. 3. A–G) SEM images of pure HA (A, D), HA/TET-1 (B, E), and HA/QUE-1 (C, G). HA/TET-1 and HA/QUE-1 indicate that tetracycline and quercetin ethanol solutions, respectively, were used at 1 mg/mL. H–J) Elemental mapping of the pure HA particle surface (H), HA/TET-1 particle surface (I), and HA/QUE-1 particle surface (J) presented for Ca P, O and C. K–M) EDX spectra of the pure HA (K), HA/TET-1 (L) and HA/QUE-1 (M) powders.

Table 2
The elemental composition of the pure HA, HA/TET-1 and HA/QUE-1 powders was estimated from EDS analysis. HA/TET-1 and HA/QUE-1 indicate that tetracycline and quercetin ethanol solutions, respectively, were used at 1 mg/mL.

Sample	Atomic Composition (%)			
	Ca	P	O	C
HA	20.41	12.01	48.04	19.54
HA/TET-1	18.80	11.65	47.78	21.78
HA/QUE-1	21.14	12.64	46.45	19.78

constant.

Binding constants provide a fundamental measure of the affinity of a solute to a ligand, and their determination is an important step in describing and understanding molecular interactions. The binding constant is a basic experimental parameter used in a variety of studies, such as the prediction of drug efficiency or drug interactions. In general, a large binding constant between the carrier and the drug is required to maintain a stable complex and improve bioavailability after implantation. The concentrations of tetracycline and quercetin gradually decreased in the solutions with immersed HA particles. The experiment was carried out until the residual value reached equilibrium. The adsorption amounts and removal rates of TET and QUE are shown in Table 3. Optical spectrophotometry revealed that HA particles adsorbed approximately 1.34 μg per milligram and 1.23 μg of tetracycline and quercetin, respectively.

In the case of TET, the residual concentration of the substance in the solution will reach the equilibrium state later than in the case of QUE, which is fully consistent with the obtained values of the binding constants.

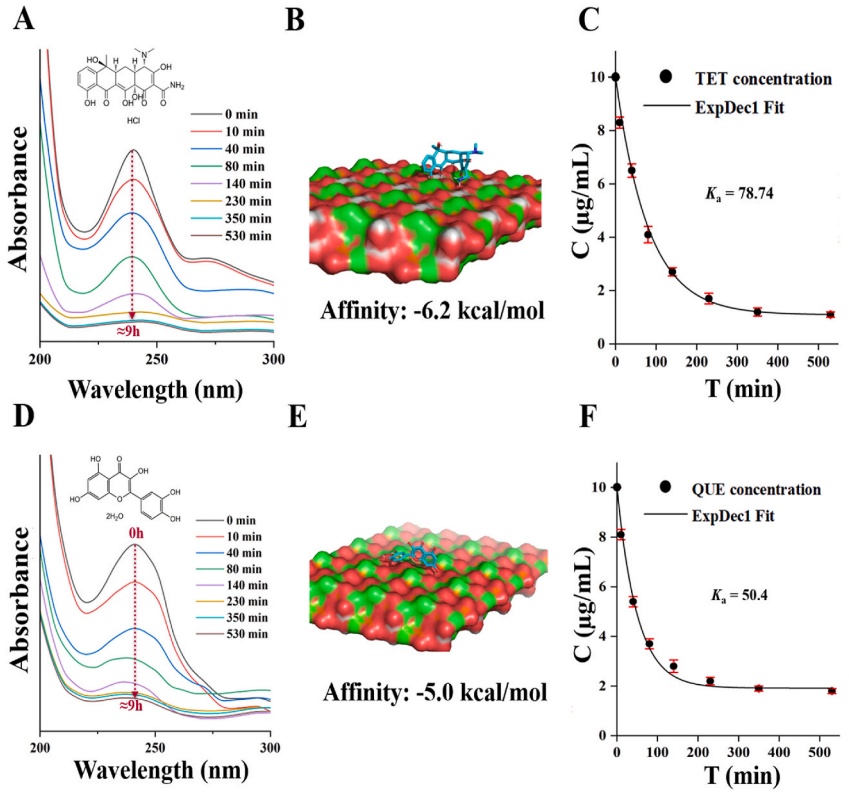

Fig. 4. UV–VIS spectra of TET (A) and QUE (D) ethanol solutions at an initial concentration of 1000 μg/mL after the HA powder was adsorbed; molecular docking affinity values of TET (B) and QUE (E) on the HA surface; experimental binding constants of TET (C) and QUE (F) on the HA surface. The adsorption experiment lasted 9 h until the system reached equilibrium.

Table 3
Adsorption characteristics and predicted equilibrium constants of TET and QUE on the HA surface. The initial substance concentration in the ethanol solutions was 10 μg/mL in the experimental settings.

Substance	Average adsorption amount (μg/mg)	Adsorption rate (%)	Ki (μM)	Ka(pred) (μM^{-1})
TET	1.34	89	28.68	0.035
QUE	1.23	82	217.18	0.005

All these observable effects could be explained by the chemical structure of tetracycline, which contains multiple functional groups that are able to interact with the HA surface through a combination of electrostatic, hydrogen bonding, and van der Waals interactions. Quercetin, on the other hand, has a simpler chemical structure and fewer functional groups that can interact with the HA surface.

3.3. Molecular docking

In our study, the experimental binding constants were compared with the binding affinities of tetracycline hydrochloride and quercetin dihydrate to the HA surface, which were calculated via molecular docking (Fig. 4B and E). Molecular docking is a widely known computational method that can be used to predict the binding affinity of small molecules to a target protein or biomolecule.

The binding constants have been calculated via molecular docking because this widely known computational method can be used to predict the binding affinity of small molecules for a target protein or biomolecule. TET and QUE are two small molecules that have been shown to have potential therapeutic effects, and their binding affinity to HA is of interest for understanding their potential as drug candidates.

Our research revealed that TET exhibited greater affinity for HA than did QUE. This was due to the lower Gibbs free energy of binding ($\Delta G = -6.2$ kcal/mol) for TET than for QUE ($\Delta G = -5.0$ kcal/mol). Gibbs free energy is a thermodynamic parameter that describes the energy change that occurs when a system undergoes a chemical reaction. In the case of molecular docking, ΔG can be used to estimate the strength of the interaction between the receptor and the ligand. The lower ΔG value for TET indicates that it has a stronger binding affinity to HA. This finding correlates with the experimental results, where TET has been found to have a higher

binding constant to HA than does QUE. The higher binding affinity value of TET to HA suggests that TET may be a more effective drug candidate for applications such as drug delivery and bone regeneration.

Our studies revealed that TET has a greater binding constant to HA ($K_a = 78.74$ (μg/mL)$^{-1}$) than to QUE ($K_a = 50.4$ (μg/mL)$^{-1}$) and a lower dissociation constant (Fig. 4C and F). This means that TET is removed from the solution more slowly and that equilibrium is reached later (but with tighter binding). In practice, the absorbance values practically do not change after 230 min for QUE and after 350 min for TET (Fig. 4A and D).

The results obtained from the adsorption experiments and molecular docking could be explained by the chemical structure of tetracycline, which contains multiple functional groups able to interact with the HA surface through a combination of electrostatic, hydrogen bonding, and van der Waals interactions. Quercetin, on the other hand, has a simpler chemical structure and fewer functional groups that can interact with the HA surface.

3.4. Antibacterial activity

Fig. 5A shows the antibacterial activity of the biocidal powders. The samples were examined via the disk diffusion method using *E. faecalis* and *S. aureus*. As shown in Fig. 5B, the inhibition zone revealed that HA particles loaded with TET from concentrated solutions (HA/TET-1) had strong antibacterial activity against 2 g-positive bacterial strains, *S. aureus* and *E. faecalis*. Notably, tetracycline and quercetin bind to HA at ratios of 1.34 μg per 1 mg of HA and 1.23 μg per 1 mg of HA, respectively. According to the literature [47–49], most gram-positive bacteria are sensitive to a TET concentration of 1 μg/mL, whereas most gram-negative bacteria are sensitive to 1–25 μg/mL TET. Quercetin also inhibits the growth of various bacterial isolates, including *Escherichia coli* and *Staphylococcus aureus,* with minimum inhibitory concentrations (MICs) ranging from 20 to 400 mg/mL [50]. Since we used 100 μg of the composites, the resulting concentration that inhibited bacterial growth was below the specified limit. This finding could prove the effectiveness of tetracycline as an additional component that gives hydroxyapatite the desired antibacterial properties. For HA powders with low concentrations of tetracycline and quercetin, no zone of inhibition was observed. The diameters of the inhibition zones of HA/TET-1 against *S. aureus* and *E. faecalis* (region 3) are 15 and 11 mm, respectively. For sample HA/TET-2 (region 4), the inhibition zone diameters are approximately 7 and 2 mm, respectively. In comparison, the HA sample taken as a control with quercetin (region 6) did not show antibacterial activity against either strain. This could be related to a decrease in the amount of quercetin adsorbed on HA particles [51].

3.5. Cytotoxicity

Since biomaterials for bone tissue restoration should have not only bactericidal properties but also osteoinductive potential, the biocompatibility of the obtained powders was tested using C2C12. The choice of TET is because this antibiotic is well studied and has been on the world market for a long time [51,52]. The choice of QUE is because it is not hemolytic [53,54]. Moreover, it rather exhibits hemolysis inhibition properties. At a concentration of 10 μg/mL, quercetin inhibited hemolysis by 35.5 %, ranking third among the tested flavonoids for this effect1. Additionally, quercetin has been shown to reduce hemolytic activity in the context of bacterial infections, indicating its protective role against erythrocyte lysis23. Overall, quercetin has beneficial effects on red blood cells rather than causing hemolysis [53].

The mouse myoblast C2C12 cell line is known to differentiate into myoblasts with further potential to differentiate into osteoblasts [54]. The viability of C2C12 cells treated with biocidal powders was confirmed by acridine orange/propidium iodide staining (Fig. 6 A). The fluorescent dye acridine orange (AO) can bind to nucleic acids within cells, causing altered spectral emission [55]. Double-stranded DNA, which is a sign of a living system, is colored green by AO, whereas damaged DNA is colored red [56]. Another

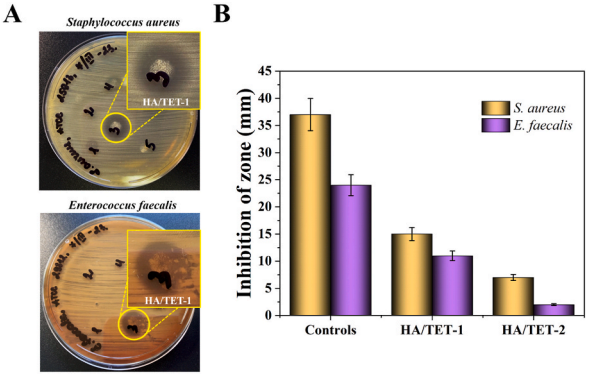

Fig. 5. (A) Antibacterial activity of HA powders with tetracycline ethanol solutions: 1 - tetracycline (500 μg/mL), 2 - tetracycline (10 μg/mL), 3 - tetracycline (1 mg/mL), 4 - tetracycline (100 μg/mL), and 5 - tetracycline (1 μg/mL). (B) Inhibition zones of *S. aureus* and *E. faecalis* were treated with two samples of HA with tetracycline (HA/TET-1 and HA/TET-2, respectively; tetracycline ethanol solutions were used at 1000 μg/mL and 100 μg/mL).

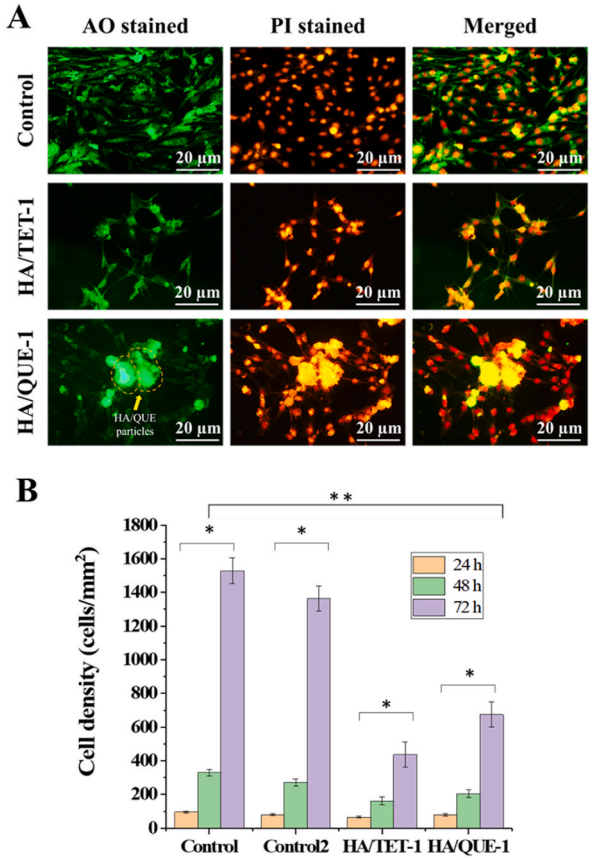

Fig. 6. (A) Fluorescence microscopy images of C2C12 cells treated with HA/TET-1 and HA/QUE-1 samples after 24 h of cultivation. The green fluorescence indicates viable cells, and the red fluorescence indicates the viable nucleus of cells. (B) Cell density (number of cells/mm^2) of C2C12 cells cultured for 24 h, 48 h and 72 h in the presence of the control, HA/TET-1 and HA/QUE-1 samples. Mean ± SE, *P < 0.05 (one-way ANOVA). The samples were tested per area type, and three independent experiments were conducted. Glass was used as a control, and pure HA particles were used as a control2. $^{**}p < 0.05$, $n = 3$.

dye that binds to nucleic acids, propidium iodide (PI), always fluoresces with an orange–red color [57]. In the case of HA adsorbed on its surface of tetracycline (HA/TET-1), prominent red fluorescence could be visualized, possibly due to the penetration of PI stain through the damaged cell membrane. This may be due to the diffusion of tetracycline through the cell membrane [58].

Fig. 6B shows that there was no significant difference in the cellular density of the control sample. In contrast, in HA/TET-1 and HA/QUE-1, there was a significant decrease (P < 0.05) in the number of C2C12 cells compared with that in the control sample. However, the cell density of the HA/QUE-1 sample was greater than that of the HA/TET-1 sample. In addition, the cell viability for all the samples was high even after contact with the HA/TET-1 and HA/QUE-1 samples. These results are also consistent with the literature data. Researchers have repeatedly shown that HA itself is not cytotoxic [59,61]. However, HA particles are capable of adsorbing nutrients from the medium and are hygroscopic, which may slightly reduce cell growth in control 2. It has also been demonstrated that the addition of components such as tetracycline and quercetin to biomaterials does not significantly increase cytotoxicity in relation to mouse and human fibroblasts and osteoblast-like cells [60–64]. In our study, we confirmed the absence of cytotoxicity for the HA/TET and HA/QUE systems.

4. Conclusions

In this work, we analyzed the adsorption of tetracycline and quercetin on the surface of hydroxyapatite. The charge of HA particles changes from −14.4 mV to +6.1 mV upon adsorption of a concentrated solution of tetracycline and to 5.4 mV for adsorption of quercetin. The results of the antibacterial tests revealed that the HA samples with tetracycline had high antibacterial activity against 2 gram-positive bacteria: *S. aureus* and *E. faecalis*. Composites with tetracycline and quercetin molecules adsorbed on the surface exhibit antibacterial activity at much lower concentrations than the same substances in unbound form in solution. In addition, the results of the cell experiments revealed that HA composites with tetracycline and quercetin have good biocompatibility.

Our study also provides important insights into the use of TET and QUE in medical applications. Our findings revealed that TET has greater binding affinity to HA than does QUE, likely due to its lower Gibbs free energy of binding. These results are consistent with

experimental data, where we have shown that TET has a larger binding constant to HA than does QUE. These findings suggest that TET may be a more effective drug candidate for applications such as drug delivery and bone regeneration and highlight the potential of molecular docking as a tool for drug discovery and biomaterial development.

CRediT authorship contribution statement

Anastasiia M. Isakova: Writing – original draft, Visualization, Validation, Investigation, Formal analysis. **Maxim A. Kutyrev:** Writing – original draft, Visualization, Validation, Investigation, Formal analysis. **Aleksandra S. Kudasheva:** Validation, Investigation. **Elizaveta V. Rogacheva:** Methodology, Investigation, Formal analysis. **Lyudmila A. Kraeva:** Writing – review & editing, Supervision, Project administration, Methodology, Investigation, Conceptualization. **Sergey Shityakov:** Writing – original draft, Supervision, Investigation, Formal analysis. **Mikhail V. Zhukov:** Writing – original draft, Investigation. **Sviatlana A. Ulasevich:** Writing – review & editing, Supervision, Project administration, Methodology, Investigation, Funding acquisition, Conceptualization. **Ekaterina V. Skorb:** Writing – review & editing, Supervision, Resources, Project administration, Conceptualization.

Data availability statement

Data will be made available on request.

Ethical statement

This study did not involve human or animal subjects, and thus, no ethical approval was required.

Declaration of competing interest

The authors declare that they have no known competing financial interests or personal relationships that could have appeared to influence the work reported in this paper.

Acknowledgments

This research was supported by Russian Science Foundation grant no. 19-79-10244. The authors acknowledge the Priority 2030 Program for infrastructural support.

References

[1] A. Ali, A. Andriyana, Properties of multifunctional composite materials based on nanomaterials: a review, RSC Adv. 10 (28) (2020), https://doi.org/10.1039/c9ra10594h.
[2] H.N. Abdelhamid, An introductory review on advanced multifunctional materials, Heliyon 9 (7) (2023) e18060, https://doi.org/10.1016/j.heliyon.2023.e18060.
[3] J. Xue, X. Wang, E. Wang, T. Li, J. Chang, C. Wu, Bioinspired multifunctional biomaterials with hierarchical microstructure for wound dressing, Acta Biomater. 100 (2019), https://doi.org/10.1016/j.actbio.2019.10.012.
[4] B.K. Shanbhag, C. Liu, G.C. Pradeep, T. Younas, K.K.Y. Hu, A.J. Fulcher, W.B. Struwe, D. Steer, G. Dumsday, I.S. Harper, P. Kukura, V.S. Haritos, L. He, Custom design of protein particles as multifunctional biomaterials, Adv. Funct. Mater. 32 (2) (2022), https://doi.org/10.1002/adfm.202108039.
[5] S.G. Rees, D.T. Hughes Wassell, G. Embery, Interaction of glucuronic acid and iduronic acid-rich glycosaminoglycans and their modified forms with hydroxyapatite, Biomaterials 23 (2) (2002), https://doi.org/10.1016/S0142-9612(01)00130-2.
[6] Y. Han, X. Wang, H. Dai, S. Li, Nanosize and surface charge effects of hydroxyapatite nanoparticles on red blood cell suspensions, ACS Appl. Mater. Interfaces 4 (9) (2012), https://doi.org/10.1021/am300992x.
[7] Z. Buchwald, M. Szołyga, J. Zwolińska, B. Marciniec, A. Voelkel, Surface modification of hydroxyapatite with polyhedral oligomeric silsesquioxane, React. Funct. Polym. 170 (2022), https://doi.org/10.1016/j.reactfunctpolym.2021.105131.
[8] D. Ubele-Kalnina, M. Nakamura, K.A. Gross, Inter-laboratory study on measuring the surface charge of electrically polarized hydroxyapatite, J. Funct. Biomater. 14 (2) (2023), https://doi.org/10.3390/jfb14020100.
[9] J. Henkel, M.A. Woodruff, D.R. Epari, R. Steck, V. Glatt, I.C. Dickinson, P.F.M. Choong, M.A. Schuetz, Di W. Hutmacher, Bone regeneration based on tissue engineering conceptions-A 21st century perspective, Bone Research 1 (2013), https://doi.org/10.4248/BR201303002.
[10] C. Wang, W. Huang, Y. Zhou, L. He, Z. He, Z. Chen, X. He, S. Tian, J. Liao, B. Lu, Y. Wei, M. Wang, 3D printing of bone tissue engineering scaffolds, Bioact. Mater. 5 (1) (2020), https://doi.org/10.1016/j.bioactmat.2020.01.004.
[11] H. Shi, Z. Zhou, W. Li, Y. Fan, Z. Li, J. Wei, Hydroxyapatite based materials for bone tissue engineering: a brief and comprehensive introduction, Crystals 11 (Issue 2) (2021), https://doi.org/10.3390/cryst11020149.
[12] D.E. Radulescu, O.R. Vasile, E. Andronescu, A. Ficai, Latest research of doped hydroxyapatite for bone tissue engineering, Int. J. Mol. Sci. 24 (Issue 17) (2023), https://doi.org/10.3390/ijms241713157.
[13] S. Lara-Ochoa, W. Ortega-Lara, C.E. Guerrero-Beltrán, Hydroxyapatite nanoparticles in drug delivery: physicochemistry and applications, Pharmaceutics 13 (Issue 10) (2021), https://doi.org/10.3390/pharmaceutics13101642.
[14] N.A.A. Halim, M.Z. Hussein, M.K. Kandar, Nanomaterials-upconverted hydroxyapatite for bone tissue engineering and a platform for drug delivery, Int. J. Nanomed. 16 (2021), https://doi.org/10.2147/IJN.S298936.
[15] H. Chouirfa, H. Bouloussa, V. Migonney, C. Falentin-Daudré, Review of titanium surface modification techniques and coatings for antibacterial applications, Acta Biomater. 83 (2019), https://doi.org/10.1016/j.actbio.2018.10.036.
[16] K. Sinulingga, M. Sirait, N. Siregar, M.E. Doloksaribu, Investigation of antibacterial activity and cell viability of Ag/Mg and Ag/Zn Co-doped hydroxyapatite derived from natural limestone, ACS Omega 6 (49) (2021), https://doi.org/10.1021/acsomega.1c05921.
[17] S. Sekaran, A. Roy, L. Thangavelu, Re-appraising the role of flavonols, flavones and flavonones on osteoblasts and osteoclasts- A review on its molecular mode of action, Chem. Biol. Interact. 355 (2022), https://doi.org/10.1016/j.cbi.2022.109831.

[18] Y. Li, S. Wang, Y. Zhang, R. Han, W. Wei, Enhanced tetracycline adsorption onto hydroxyapatite by Fe(III) incorporation, J. Mol. Liq. 247 (2017), https://doi.org/10.1016/j.molliq.2017.09.110.

[19] S.K. Wong, K.Y. Chin, S. Ima-Nirwana, Quercetin as an agent for protecting the bone: a review of the current evidence, Int. J. Mol. Sci. 21 (17) (2020), https://doi.org/10.3390/ijms21176448.

[20] H.W. Kim, J.C. Knowles, H.E. Kim, Hydroxyapatite/poly(ε-caprolactone) composite coatings on hydroxyapatite porous bone scaffold for drug delivery, Biomaterials 25 (7–8) (2004), https://doi.org/10.1016/j.biomaterials.2003.07.003.

[21] L.C. Rusu, I.A. Nedelcu, M. Georgiana Albu, M. Sonmez, G. Voicu, M. Radulescu, D. Ficai, A. Ficai, M.L. Negrutiu, C. Sinescu, Tetracycline loaded collagen/hydroxyapatite composite materials for biomedical applications, J. Nanomater. 2015 (2015), https://doi.org/10.1155/2015/361969.

[22] D. Predoi, S.L. Iconaru, M.V. Predoi, N. Buton, Development of novel tetracycline and ciprofloxacin loaded silver doped hydroxyapatite suspensions for biomedical applications, Antibiotics 12 (1) (2023), https://doi.org/10.3390/antibiotics12010074.

[23] L. Forte, P. Torricelli, E. Boanini, M. Gazzano, K. Rubini, M. Fini, A. Bigi, Antioxidant and bone repair properties of quercetin-functionalized hydroxyapatite: an in vitro osteoblast-osteoclast-endothelial cell co-culture study, Acta Biomater. 32 (2016), https://doi.org/10.1016/j.actbio.2015.12.013.

[24] F. Malvano, A.M.I. Montone, F. Capuano, C. Colletti, N. Roveri, D. Albanese, R. Capparelli, Effects of active alginate edible coating enriched with hydroxyapatite-quercetin complexes during the cold storage of fresh chicken fillets, Food Packag. Shelf Life 32 (2022), https://doi.org/10.1016/j.fpsl.2022.100847.

[25] A.M.I. Montone, M. Papaianni, F. Malvano, F. Capuano, R. Capparelli, D. Albanese, Lactoferrin, quercetin, and hydroxyapatite act synergistically against pseudomonas fluorescens, Int. J. Mol. Sci. 22 (17) (2021), https://doi.org/10.3390/ijms22179247.

[26] M.G. Salvador, G.E. Daniel, R.R. Jesús Manuel, Sternoclavicular osteomyelitis secondary to Enterococcus faecalis neck abscess. Case report, Enfermedades Infecc. Microbiol. 42 (1) (2022).

[27] A. Krzysztofiak, et al., Clinical report and predictors of sequelae of 319 cases of pediatric bacterial osteomyelitis, Sci. Rep. 12 (1) (2022), https://doi.org/10.1038/s41598-022-19208-2.

[28] W. Feng, L. Mu-Sen, L. Yu-Peng, Q. Yong-Xin, A simple sol-gel technique for preparing hydroxyapatite nanopowders, Mater. Lett. 59 (8–9) (2005), https://doi.org/10.1016/j.matlet.2004.08.041.

[29] Clinical and Laboratory Standards Institute (CLSI), Performance Standards for Antimicrobial Susceptibility Testing, 33rd ed., Clinical and Laboratory Standards Institute, USA, 2023. CLSI supplement M100 (ISBN 978-1-68440-170-3 [Print]; ISBN 978-1-68440-171-0 [Electronic]).

[30] E. Matuschek, D.F.J. Brown, G. Kahlmeter, Development of the EUCAST disk diffusion antimicrobial susceptibility testing method and its implementation in routine microbiology laboratories, Clin. Microbiol. Infection 20 (4) (2014) O255–O266.

[31] J.M. Schurr, D.P. Rangel, S.R. Aragon, A contribution to the theory of preferential interaction coefficients, Archived October 11, 2007, at the Wayback Machine Biophysical Journal 89 (2005) 2258–2276.

[32] E.C. Reynolds, A. Wong, Effect of adsorbed protein on hydroxyapatite zeta potential and Streptococcus mutans adherence, Infect. Immun. 39 (3) (1983), https://doi.org/10.1128/iai.39.3.1285-1290.1983.

[33] J. Latocha, M. Wojasiński, O. Janowska, U. Chojnacka, S. Gierlotka, T. Ciach, P. Sobieszuk, Morphology-controlled precipitation/remodeling of plate and rod-shaped hydroxyapatite nanoparticles, AIChE J. 68 (12) (2022), https://doi.org/10.1002/aic.17897.

[34] M. Beiranvand, S. Farhadi, A. Mohammadi-Gholami, Adsorptive removal of tetracycline and ciprofloxacin drugs from water by using a magnetic rod-like hydroxyapatite and MIL-101(Fe) metal-organic framework nanocomposite, RSC Adv. 12 (53) (2022), https://doi.org/10.1039/d2ra06213e.

[35] A. Naqshbandi, A. Rahman, Sodium doped hydroxyapatite: synthesis, characterization and zeta potential studies, Mater. Lett. 312 (2022), https://doi.org/10.1016/j.matlet.2022.131698.

[36] A. Doostmohammadi, A. Monshi, R. Salehi, M.H. Fathi, S. Karbasi, U. Pieles, A.U. Daniels, Preparation, chemistry and physical properties of bone-derived hydroxyapatite particles having a negative zeta potential, Mater. Chem. Phys. 2 (3) (2012) 446–452, https://doi.org/10.1016/j.matchemphys.2011.11.051, 132.

[37] A.A.H. Faisal, D.N. Ahmed, M. Rezakazemi, N. Sivarajasekar, G. Sharma, Cost-effective composite prepared from sewage sludge waste and cement kiln dust as permeable reactive barrier to remediate simulated groundwater polluted with tetracycline, J. Environ. Chem. Eng. 9 (3) (2021), https://doi.org/10.1016/j.jece.2021.105194.

[38] S. Rahman, K.H. Maria, M.S. Ishtiaque, A. Nahar, H. Das, S.M. Hoque, Evaluation of a novel nanocrystalline hydroxyapatite powder and a solid hydroxyapatite/Chitosan-Gelatin bioceramic for scaffold preparation used as a bone substitute material, Turk. J. Chem. 44 (4) (2020), https://doi.org/10.3906/KIM-1912-40.

[39] S.M. Rabiee, Development of hydroxyapatite bone cement for controlled drug release via tetracycline hydrochloride, Bull. Mater. Sci. 36 (1) (2013), https://doi.org/10.1007/s12034-013-0424-9.

[40] L. Forte, P. Torricelli, E. Boanini, M. Gazzano, K. Rubini, M. Fini, A. Bigi, Antioxidant and bone repair properties of quercetin-functionalized hydroxyapatite: an in vitro osteoblast-osteoclast-endothelial cell co-culture study, Acta Biomater. 32 (2016), https://doi.org/10.1016/j.actbio.2015.12.013.

[41] L. Yang, W. Zhong, J. Cui, Z. Wei, W. Wei, Enhanced removal of Cu(II) ions from aqueous solution by poorly crystalline hydroxyapatite nanoparticles, J. Dispersion Sci. Technol. 37 (7) (2016), https://doi.org/10.1080/01932691.2015.1077140.

[42] W. Wei, X. Zhang, J. Cui, Z. Wei, Interaction between low molecular weight organic acids and hydroxyapatite with different degrees of crystallinity, Colloids Surf. A Physicochem. Eng. Asp. 392 (1) (2011), https://doi.org/10.1016/j.colsurfa.2011.09.034.

[43] S. Koutsopoulos, Synthesis and characterization of hydroxyapatite crystals: a review study on the analytical methods, J. Biomed. Mater. Res.: An Official Journal of The Society for Biomaterials, The Japanese Society for Biomaterials, and The Australian Society for Biomaterials and the Korean Society for Biomaterials 62 (4) (2002) 600–612, https://doi.org/10.1002/jbm.10280.

[44] P. Papan, J. Kantapan, P. Sangthong, P. Meepowpan, N. Dechsupa, Iron (III)-Quercetin complex: synthesis, physicochemical characterization, and MRI cell tracking toward potential applications in regenerative medicine, Contrast Media Mol. Imaging (2020) 8877862, https://doi.org/10.1155/2020/8877862.

[45] A. Brangule, K.A. Gross, Importance of FTIR spectra deconvolution for the analysis of amorphous calcium phosphates, in: IOP Conference Series: Materials Science and Engineering, vol. 77, IOP Publishing, 2015, March 012027, https://doi.org/10.1088/1757-899X/77/1/012027, 1.

[46] D. Predoi, S.L. Iconaru, M.V. Predoi, N. Buton, Development of novel tetracycline and ciprofloxacin loaded silver doped hydroxyapatite suspensions for biomedical applications, Antibiotics 12 (1) (2022) 74, https://doi.org/10.3390/antibiotics12010074.

[47] D.N. Misra, Adsorption and orientation of tetracycline on hydroxyapatite, Calcif. Tissue Int. 48 (1991) 362–367, https://doi.org/10.1007/BF02556156.

[48] D. Predoi, C.L. Popa, P. Chapon, A. Groza, S.L. Iconaru, Evaluation of the antimicrobial activity of different antibiotics enhanced with silver-doped hydroxyapatite thin films, Materials 9 (9) (2016), https://doi.org/10.3390/ma9090778.

[49] J. Wang, N. Cai, V. Chan, H. Zeng, H. Shi, Y. Xue, F. Yu, Antimicrobial hydroxyapatite reinforced-polyelectrolyte complex nanofibers with long-term controlled release activity for potential wound dressing application, Colloids Surf. A Physicochem. Eng. Asp. 624 (2021), https://doi.org/10.1016/j.colsurfa.2021.126722.

[50] O.S. Adeyemi, C. Ebugosi, O.B. Akpor, H.F. Hetta, S. Al-Rashed, D.A. Otohinoyi, G.E.S. Batiha, Quercetin caused redox homeostasis imbalance and activated the kynurenine pathway, Biology 9 (8) (2020) 219, https://doi.org/10.3390/biology9080219.

[51] M. Dapporto, M. Tavoni, E. Restivo, F. Carella, G. Bruni, L. Mercatali, L. Visai, A. Tampieri, M. Iafisco, S. Sprio, Strontium-doped apatitic bone cements with tunable antibacterial and antibiofilm ability, Front. Bioeng. Biotechnol. 10 (2022), https://doi.org/10.3389/fbioe.2022.969641.

[52] M. García-Castro, F. Sarabia, A. Díaz-Morilla, J.M. López-Romero, Approved antibacterial drugs in the last 10 years: from the bench to the clinic, Exploration of Drug Science 1 (3) (2023) 180–209, https://doi.org/10.37349/eds.2023.00013.

[53] K. Men, X. Duan, X. Wei Wei, M. Ling Gou, M. Juan Huang, L. Juan Chen, Y. Quan Wei, Nanoparticle-delivered quercetin for cancer therapy, Anti Cancer Agents Med. Chem. 14 (6) (2014) 826–832.

[54] S. Wang, J. Yao, B. Zhou, J. Yang, M.T. Chaudry, M. Wang, F. Xiao, Y. Li, W. Yin, Bacteriostatic effect of quercetin as an antibiotic alternative in vivo and its antibacterial mechanism in vitro, J. Food Protect. 81 (1) (2018), https://doi.org/10.4315/0362-028X.JFP-17-214.

[55] M. Czuban, M.W. Kulka, L. Wang, A. Koliszak, K. Achazi, C. Schlaich, A. Trampuz, Titanium coating with mussel inspired polymer and bio-orthogonal chemistry enhances antimicrobial activity against Staphylococcus aureus, Mater. Sci. Eng. C 116 (2020) 111109, https://doi.org/10.1016/j.msec.2020.111109.

[56] D. Denton, S. Kumar, Using the vital dye acridine orange to detect dying cells in drosophila, Cold Spring Harbor Protocols 2015 (6) (2015), https://doi.org/10.1101/pdb.prot086207.
[57] Z. Darzynkiewicz, D. Evenson, J. Kapuscinski, M.R. Melamed, Denaturation of RNA and DNA in situ induced by acridine orange, Experimental cell research 148 (1) (1983) 31–46. https://pubmed.ncbi.nlm.nih.gov/6195003/.
[58] H.G.J.M. Kuypers, A.M. Huisman, Fluorescent neuronal tracers, in: Advances in Cellular Neurobiology, vol. 5, Elsevier, 1984, pp. 307–340, https://doi.org/10.1016/B978-0-12-008305-3.50014-3.
[59] M. Sirait, K. Sinulingga, N. Siregar, M.E. Doloksaribu, Amelia, Characterization of hydroxyapatite by cytotoxicity test and bending test, J. Phys. Conf. 2193 (1) (2022), https://doi.org/10.1088/1742-6596/2193/1/012039.
[60] C.C. Coelho, L. Grenho, P.S. Gomes, P.A. Quadros, M.H. Fernandes, Nano-hydroxyapatite in oral care cosmetics: characterization and cytotoxicity assessment, Sci. Rep. 9 (1) (2019), https://doi.org/10.1038/s41598-019-47491-z.
[61] A. Andrew, I. Ervina, H. Agusnar, In vitro chitosan hydrogel based tetracycline cytotoxicity test on fibroblast viability. https://doi.org/10.2991/idsm-17.2018.36, 2018.
[62] J. Rivadeneira, A.L. di Virgilio, M.C. Audisio, A.R. Boccaccini, A.A. Gorustovich, Evaluation of antibacterial and cytotoxic effects of nano-sized bioactive glass/collagen composites releasing tetracycline hydrochloride, J. Appl. Microbiol. 116 (6) (2014), https://doi.org/10.1111/jam.12476.
[63] M. Catauro, F. Papale, F. Bollino, S. Piccolella, S. Marciano, P. Nocera, S. Pacifico, Silica/quercetin sol-gel hybrids as antioxidant dental implant materials, Sci. Technol. Adv. Mater. 16 (3) (2015), https://doi.org/10.1088/1468-6996/16/3/035001.
[64] F. Ao, X. Luo, W. Shen, X. Ge, P. Li, Y. Zheng, S. Wu, Y. Mao, Y. Luo, Multifunctional electrospun membranes with hydrophilic and hydrophobic gradients property for wound dressing, Colloids Surf. B Biointerfaces 225 (2023), https://doi.org/10.1016/j.colsurfb.2023.113276.